small NANO MICRO

Lab-on-Chip Devices

Surface-Tension-Driven Gradient Generation in a Fluid Stripe for Bench-Top and Microwell Applications

*Matthew J. Hancock, Jiankang He, João F. Mano, and Ali Khademhosseini**

A *simple and inexpensive method is presented employing passive mechanisms to generate centimeters-long gradients of molecules and particles in under a second with only a coated glass slide and a micropipette. A drop of solution is pipetted onto a fluid stripe held in place on a glass slide by a hydrophobic boundary. The resulting difference in curvature pressure drives the flow and creates a concentration gradient by convection. Experiments and theoretical models characterize the flows and gradient profiles and their dependence on the fluid volumes, properties, and stripe geometry. A bench-top rapid prototyping method is outlined to allow the user to design and fabricate the coated slides using only tape and hydrophobic spray. The rapid prototyping method is compatible with microwell arrays, allowing soluble gradients to be applied to cells in shear-protected microwells. The method's simplicity makes it accessible to virtually any researcher or student and its use of passive mechanisms makes it ideal for field use and compatible with point-of-care and global health initiatives.*

1. Introduction

Material, chemical and biological gradients have found widespread use in biotechnology and materials science for applications such as diagnostics, fundamental studies on biological processes, and material screening.[1] A host of techniques, generally involving microfluidic devices and auxiliary apparatus, exist to create chemical and material gradients

Dr. M. J. Hancock,[†] Dr. J. He,[†] Prof. A. Khademhosseini
Center for Biomedical Engineering
Department of Medicine
Brigham and Women's Hospital
Harvard Medical School
65 Landsdowne Street
Cambridge, MA 02139, USA

Dr. J. He
State Key Laboratory of Manufacturing Systems Engineering
Xi'an Jiaotong University
Xi'an, Shaanxi 710049, China

Prof. J. F. Mano
3Bs Research Group (Biomaterials, Biodegradables, and Biomimetics)
Department of Polymer Engineering
University of Minho
Headquarters of the European Institute of Excellence on Tissue Engineering and Regenerative Medicine
AvePark, São Cláudio do Barco, 4806-909 Taipas, Guimarães, Portugal

[†] These authors contributed equally.

Prof. J. F. Mano
PT Government Associated Laboratory
Institute for Biotechnology and Bioengineering (IBB)
Guimarães, Portugal

Prof. A. Khademhosseini
Partners Research Building
Room 252, 65 Landsdowne Street
Cambridge, MA 02139, USA
E-mail: alik@rics.bwh.harvard.edu

Prof. A. Khademhosseini
Wyss Institute for Biologically Inspired Engineering
Harvard University
Boston, MA 02115, USA

Prof. A. Khademhosseini
Harvard-MIT Division of Health Sciences and Technology
Massachusetts Institute of Technology
Cambridge, MA 02139, USA

DOI: 10.1002/smll.201002088

on 2D surfaces and in 3D, for example, the classic tree-like gradient generator,[2] a commercial gradient maker (or equivalently, syringe pumps in tandem),[3] and convection flows in microchannels.[4–6]

A growing need exists for microfluidic devices that are portable, low-power, inexpensive, simple to use, storable, and disposable. Such characteristics are essential for point-of-care devices suitable for global health initiatives.[7] Experiments with hazardous or fouling materials necessitate the use of disposable devices, while those involving many repetitions require inexpensive devices and fast and simple protocols. Moreover, costs associated with fabrication, whether done in-house or commercially, add significantly to overall project costs. Recently, simplified techniques have been developed for fabricating microfluidic devices,[8] actuating and directing flow,[9] and for cell patterning.[10] Existing protocols for gradient generation, even simplified approaches,[5,6,11] still generally involve microfabricated devices and additional preparation time for device assembly and setup. Design modifications require new silicon molds, leading to further expense and labor.

The gradient technique presented herein employs passive mechanisms, surface tension and diffusion, and inexpensive coated slides that can be obtained commercially or fabricated on a bench-top with inexpensive off-the-shelf components (glass slides, tape, hydrophobic spray: see **Figure 1**A). Our design employs a hydrophilic region on which fluid resides bounded by a hydrophobic coating acting like a virtual wall (Figure 1B,C). Similar designs have been used for droplet pathways[12] and continuous fluid streams[13] without physical channel walls. A concentration gradient is created when a droplet of solution is pipetted onto one end of the fluid stripe, resulting in a high local curvature pressure that drives the flow (Figure 1B,D). The flow lasts for under a second, and the diffusion necessary to achieve the desired lateral uniformity is completed in minutes. The gradient length and slope are controlled by the fluid stripe and droplet volumes. Herein, the shape and stability of static fluid stripes are reviewed, based on previous calculations.[14] Mathematical models are derived to estimate the speed of fluid motion and the shape and length of the gradients. The technique is then used to create crossing microparticle gradients along a stripe and drug gradients over seeded cells in microwell arrays.

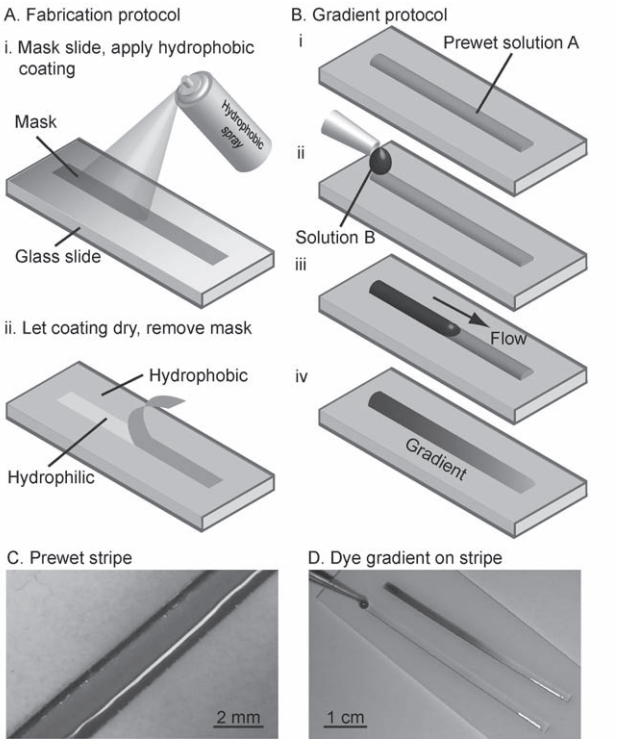

Figure 1. Fabrication and operation of gradient device. A) Fabrication protocol: i) Mask rectangular region of dimensions $W \times L$ on a glass slide and apply hydrophobic spray. ii) Allow hydrophobic spray to dry and remove mask, exposing hydrophilic stripe surrounded by hydrophobic boundary. B) Protocol for gradient generation: i) Prewet hydrophilic stripe with solution A. ii) Pipette a drop of solution B at one end of the prewet hydrophilic stripe. iii) Resulting flow spreads drop along prewet fluid and so generates a gradient. iv) The gradient solution may be left to achieve desired lateral uniformity and then be used or analyzed. C) Close-up of a static fluid stripe bounded by hydrophobic coating. D) Two fluid stripes on a coated slide, one with a dye gradient created by the gradient protocol. Droplet and prewet fluid stripe also shown.

2. Results and Discussion

2.1. Static Fluid Stripe

The shape and stability of static fluid stripes are well understood and characterized.[14,15,16] The fluid stripe height H is defined as the depth of the fluid above the hydrophilic boundary. The fluid stripes of interest have heights H, widths W, and lengths L separated by an order of magnitude, $H \ll W \ll L$, with small contact angles between the fluid and hydrophilic substrate (Figure 1C). The relative magnitudes of the gravitational and capillary forces acting on the fluid stripe are characterized by the Bond number, $\mathrm{Bo} = \rho g W^2/\sigma$, where ρ is the liquid density, g is the acceleration of gravity, and σ is the surface tension of the liquid–air meniscus. Since $\mathrm{Bo} < 1$ in the regime of interest, gravitational effects may be neglected for static stripes, which have nearly constant pressure and cylindrical cross-sections of curvature radius R (see Supporting Information (SI), Section I).[16] These near-cylindrical stripes with small contact angles are stable[14,16] and are described approximately by the geometrical relations (SI, Section I),

$$H \approx \frac{3A}{2W},\ R \approx \frac{W^3}{12A}, \tag{1}$$

where A is the area of a lateral cross-section. For a static fluid stripe, $A \approx V/L$, where V is the stripe volume. For example, for a stripe of length $L = 5$ cm, width $W = 0.2$ cm, and volume $V = 15$ µL, we have $H = 225$ µm and $R = 0.22$ cm. For these values, the height was measured with callipers to be $H = 220 \pm 10$ µm (SI, Section I). In addition, the linear relation between H and V is evident from the measured centerline intensities of stripes of fluorescent fluid (SI, Figure S1D).

small NANO MICRO

2.2. Droplet-Induced Fluid Motion

In each experiment reported herein, a droplet was brought in contact with a prewet fluid stripe and immediately and fully coalesced (Figure 1B). The local increase in curvature pressure induced a flow to bring the fluid stripe to a new equilibrium at the total volume (prewet plus droplet). Droplets of dye were added to the prewet stripe to measure the characteristic speeds of fluid motion (**Figure 2**A), which initially ranged from $U = 14$–26 cm s^{-1} for the first 100–200 ms, followed by slower flows on the order of millimeters per second lasting up to ≈1 s. The surface-tension driven flow speeds were of the same order as the capillary wave speed[16] $(\sigma/\rho R)^{1/2}$, which was 18 cm s^{-1} for our system with a prewet volume $V_w = 15$ μL of water ($R = 0.22$ cm from Equation 1). The characteristic Reynolds numbers $\rho HU/\mu$ ranged from 30 to 60; in this regime, theoretical treatments exist for small-amplitude capillary waves that are inviscid[14] or viscously damped.[16]

Due to the complex flows associated with drop coalescence,[17] the large amplitude disturbances imparted by drop addition, and the large mass rebalance that occurs as the droplet is redistributed along the stripe, we limit our treatment to scaling models of the flow speed and gradient-profile shape. The 8 independent physical parameters of the fluid system are the prewet volume V_w, droplet volume V_d, stripe width W and length L, the fluid viscosity μ and density ρ, the surface tension σ of the air–fluid interface, and gravity g. Dimensional analysis provides a reduced set of five dimensionless parameters: W/L (aspect ratio); V_d/V_w (volume ratio); V_w/LW^2 (dimensionless prewet volume); Bo = $\rho g W^2/\sigma$ (Bond number); and Ca = $\mu/(\sigma\rho W)^{1/2}$ (capillary number). Though gravitational effects, as parameterized by Bo, are negligible for the static stripe cross-sections in the regime of interest, they still affect disturbances propagating along multicentimeter-long stripes. The capillary number quantifies the relative effects of viscosity and surface tension; for this system, Ca = 0.0026. Though Ca is small, the effects of viscosity are present in this system and, in the regime of interest, damp the flow before it reaches the end of the stripe. As such, the length does not directly affect the flow or gradient profile, and the set of parameters may be reduced to four: V_d/AW, A/W^2, Bo, and Ca, where $A = V_w/L$ is the lateral cross-sectional area. Lastly, based on Equation 1 and the capillary wave speed $U \approx (\sigma/\rho R)^{1/2}$, the Reynolds number $\rho HU/\mu$ scales as Re = $(V_w/LW^2)^{3/2}$ Ca^{-1} and is not an additional independent parameter.

The flow-speed model assumes a parabolic profile with zero surface stress and no slip at the bottom. The maximum velocity is at the surface and takes the form

$$u_{max} = \frac{H^2 \Delta}{2\mu} \tag{2}$$

where Δ is the magnitude of the pressure gradient and H is the local depth. The pressure is dominated by the local curvature pressure, which scales as $p \approx \sigma/R$. R_1 is defined as the characteristic radius of curvature of the disturbance, R_0 as the curvature of the undisturbed fluid stripe, and x as the position

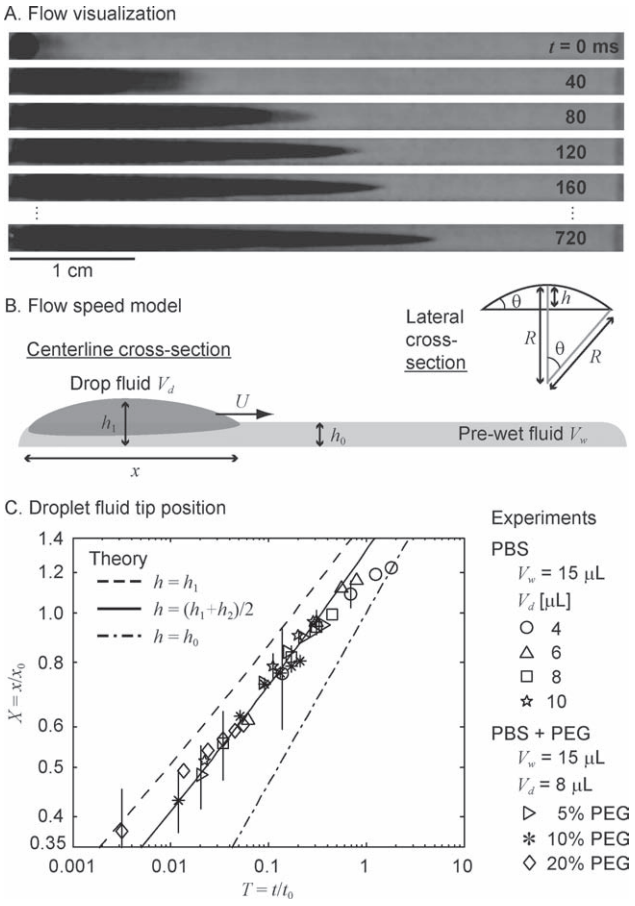

Figure 2. Speed of fluid motion. A) Consecutive frames of a 15 μL fluid stripe following the addition of a 8 μL drop of blue dye. The flow speed is initially ≈10–40 cm s^{-1} and decreases to ≈1 mm s^{-1}. Stripe length is 5 cm. B) Schematic of droplet of volume V_d spreading along a stripe of prewet volume V_w. At time t, the droplet has speed U, length x and height h_1. Inset: lateral cross-section has circular segment geometry. C) Measurements of droplet solution tip position over time in terms of dimensionless variables $X = x/x_0$ and $T = t/t_0$ (see Equation (8)) for different prewet and droplet volumes and fluids. Three versions of the speed model, Equation 5 to 7, are plotted for comparison: Equation (6) associated with the mean depth $(h_1 + h_0)/2$ gives best agreement. The data collapse indicates the appropriate scaling. Standard deviation was less than 5% of mean except where noted by error bars. PBS = phosphate buffered saline, PEG = polyethylene glycol.

of the dye tip. It may be assumed that x is also the transition length over which the curvature changes from R_1 to R_0 (an alternative choice for the transition length, R_1, is made in the SI, Section II, which produces speeds that are an order of magnitude larger than those observed). With these assumptions, the pressure gradient scales as

$$\Delta = \frac{\sigma}{x}\left(\frac{1}{R_1} - \frac{1}{R_0}\right) \tag{3}$$

The geometrical approximations in Equation 1 allow us to write R_1 and R_0 in terms of the local cross-sectional areas A_1 and A_0. The area A_0 of the undisturbed (prewet only) stripe is given by V_w/L. As the droplet volume spreads over a distance x, it flows over a fraction x/L of the prewet volume (Figure 2B), so that A_1 scales as

$$A_1 x = V_d + \frac{x}{L} V_w \tag{4}$$

Solving Equation 4 for A_1, substituting A_0 and A_1 into Equation 1 to obtain R_1 and R_0, substituting these into Equation 3, and then Equation 3 into Equation 2 gives the tip speed u_{max} (for additional details see the Mathematica script in SI Section VI). The appropriate choice for H in Equation 2 is not evident a priori; three reasonable options include h_0, $(h_1 + h_0)/2$, and h_1 (Figure 2B), which result in three speed estimates u_{max}, the reciprocals of which are integrated subject to $x(0) = 0$ to obtain implicit relations for the position $x(t)$. In terms of the dimensionless position $X = x/x_0$ and time $T = t/t_0$, we obtain for $H = h_0, (h_1 + h_0)/2, h_1$ respectively,

$$T = X^3 \tag{5}$$

$$T = \frac{1}{4}\left(X\left(9 - 6X + 4X^2\right) + \frac{3X}{1 + 2X} - 6\log(1 + 2X)\right) \tag{6}$$

$$T = \frac{3X}{1 + X} + 3X\left(3 - X + \frac{X^2}{3}\right) - 12\log(1 + X) \tag{7}$$

where the characteristic length and time scales are defined by

$$t_0 = \frac{2\mu L^5 W^5 V_d^2}{81\sigma V_w^5},\ x_0 = \frac{L V_d}{V_w}. \tag{8}$$

For an 8 μL water droplet added to a 15 μL stripe of water ($\mu = 0.01$ cm^2 s^{-1}, $\sigma = 72$ dynes cm^{-1}, where 1 dyne = 1 cm s^{-2} g^{-1}) on our stripe ($W = 0.2$ cm, $L = 5$ cm), the characteristic position and time scales are $t_0 = 290$ ms and $x_0 = 2.6$ cm, within the orders of magnitude outlined above. The three estimates of the dye-tip position are plotted in Figure 2C with our accompanying measurements in buffer and poly(ethylene glycol) (PEG) solutions. The viscosities of the various concentrations of PEG were found in the literature.[18] Since the precise time of flow initiation likely occurred between video frames and was complicated by coalescence, the time of the first frame of each set was set arbitrarily as $t = 0.01$ s, providing good data collapse. The agreement between the measurements and the model Equation 6, employing the average depth $(h_1+h_0)/2$, is reasonable (Figure 2C). The model Equation 5, associated with the shallower depth h_0, underestimates the flow speed, while Equation 7, associated with the larger depth h_1, overestimates the speed. Lastly, our estimates calculated above for the flow speed u_{max}, with $x \approx L$, scale as $u_{max} \approx (\sigma/\mu)(V_d/V_w)(V_w/LW^2)^3(W/L)$. The speed is proportional to the volume ratio and the surface tension and inversely proportional to the viscosity. For a constant fluid depth H (equivalent to constant V_w/LW, from Equation 1), $u_{max} \approx W^{-2}$, so that faster speeds are expected for narrower fluid stripes. Though the capillary number and Bond number do not appear explicitly, they affect the speed through the fluid depth and the extent of the propagating disturbance, and could help parameterize a more general speed model.

2.3. Soluble Gradient Profiles

The length and shape of soluble gradients on the fluid stripe depend on the droplet and prewet volumes, viscosity, surface tension, and molecular diffusion. Top-down views and centerline intensity profiles of gradients of fluorescent dye in buffer solution are shown in **Figure 3**A for various prewet and droplet volumes. In general, the gradient length increases with droplet volume and decreases with prewet volume. Linear centerline gradients were observed for prewet volumes of 15 and 20 μL and droplet volumes ranging from 4 to 10 μL, while more rounded (i.e., nonlinear) profiles were observed outside this range (Figure 3A, and SI, Section III.3 and Figure S8). Gradient profiles are reproducible with moderate variation (Figure 3A and SI, Figure S4), which could be reduced by improved droplet delivery (e.g., syringe pump) and fabrication (e.g., commercially coated slides).

A scaling model is derived to estimate the lengths of the final droplet plume and gradient (Figure 3B). The final fluid stripe has volume $V_w + V_d$ and depth $h = 3(V_w + V_d)/(2LW)$ based on Equation 1. The final droplet plume volume scales as $V_d \approx x_d W h$, where x_d is the plume length. Rearranging for x_d and substituting for h, we have

$$\frac{x_d}{L} = \frac{c\, V_d/V_w}{1 + V_d/V_w} \tag{9}$$

where c is a dimensionless coefficient depending on the dimensionless parameters identified above, V_d/V_w, W/L, V_w/LW^2, Bo, and Ca, as well as the Péclet number quantifying the relative magnitudes of advection and diffusion, Pe = UH/D, where D is the molecular diffusivity. Measured lengths of the final droplet plumes spanning the regime of interest collapse onto a single curve for $V_d/V_w > 0.4$ (Figure 3C). The coefficient $c(V_d/V_w) = 2.81/(1 + 0.56V_d/V_w)$ provides a good fit, even for experiments involving different concentrations of PEG. Under the idealized assumptions of a plug of droplet solution stretched by a parabolic flow, the length x_d is calculated in the SI, Section III.1. Neglecting the initial length of the plug yields $c = 35/16 = 2.19$, a reasonable estimate for moderate to small volume ratios (Figure 3C). Larger droplets form longer initial plugs, which reduces the overall length (SI, Section III.1, Equation S18). Since the initial shape and size of the droplet solution depend on the details of the coalescence, their combined effect could be included with the coefficient c in Equation (9) (SI, Section III.1). The gradient length is defined as the extent of the region over which the concentration transitions from 90% to 10%. The lengths of the most linear gradients are approximately 80% of the final droplet plume length, with an adjustment for the length of the end of the fluid stripe, which scales as the capillary length $l_c = (\sigma/\rho g)^{1/2}$ (Figure 3D).

The precise shape of the concentration profile depends on the initial droplet shape and the subsequent flow and

NANO MICRO small

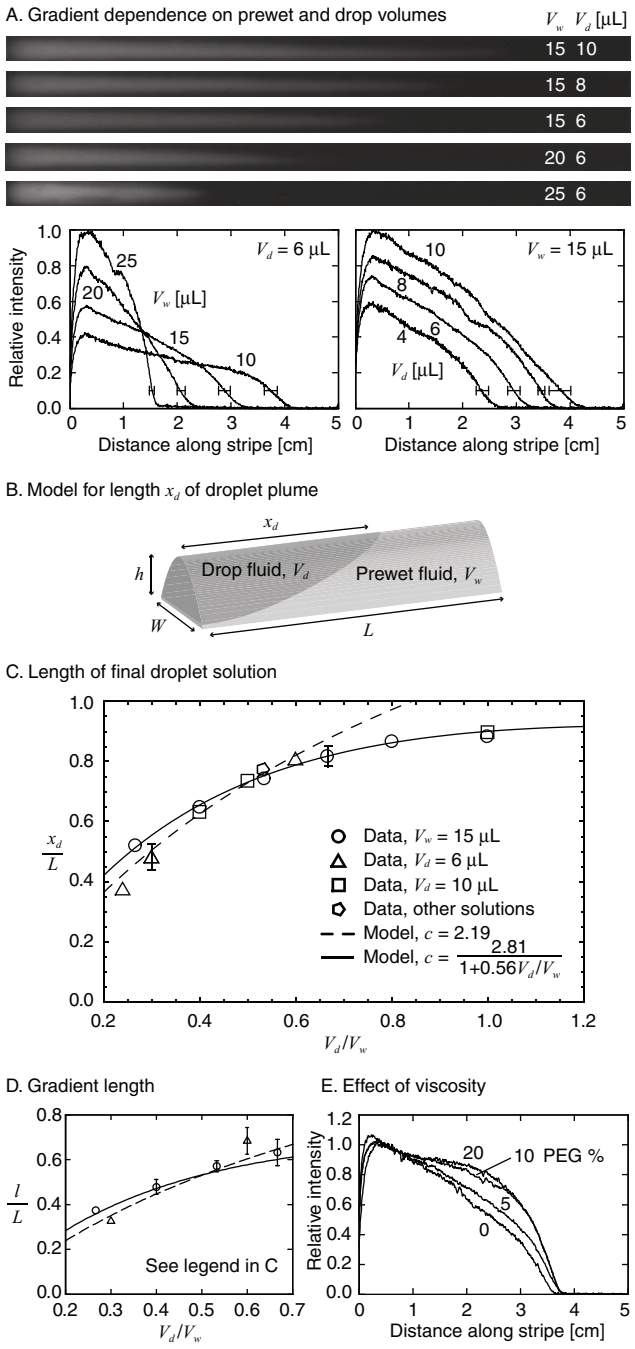

Figure 3. Length and shape of soluble gradients. A) Top-down views of gradients of fluorescent dye for various droplet and prewet volumes. Below, the corresponding centerline relative intensity profiles. Error bars indicate standard deviation over at least three repetitions. B) Schematic of scaling model for length of final droplet plume. C) Measured final droplet plume length x_d scaled by stripe length L in terms of volume ratio V_d/V_w. Scaling model Equation (9) with appropriate coefficient plotted for comparison. Other solutions incuded cell medium and PEG solutions. D) Measured linear gradient lengths in terms of the volume ratio V_d/V_w. Scaling model $l = 0.8x_d - l_c$ is plotted for comparison, where x_d is given by Equation (9) with appropriate coefficient and $l_c = 2.7$ mm is the capillary length of water. Lines and symbols correspond to the legend in (C). E) Measured centerline gradients for PEG solutions show effect of viscosity. In (C,D), experiments were repeated at least three times and the standard deviation was less than the symbol size except where noted by error bars.

mass transport. Under the idealized assumptions of a plug of droplet solution stretched by a parabolic flow, the centerline concentration takes the approximate form $\sqrt{c_1 - c_2 x/L}$ for coefficients c_1, c_2 (SI, Section III.2 and Figure S6). In the regime of interest, $U \approx 10$ cm s^{-1}, $H \approx 100$ μm, molecular diffusivity $D \approx 10^{-6}$ cm^2 s^{-1}, and the Péclet number has order of magnitude Pe ~ 10^5, indicating that the mass transport is dominated by advection. Nonlinear gradients are produced in solutions more viscous than water (Figure 3E, and SI, Section III.3 and Figure S8). These gradients still have linear portions, albeit shorter (≈0.5–1 cm), useful for biological experiments. The increased viscosity could alter the coalescence and subsequent flow. The gradient nonlinearity is not likely due to mass transport effects, since even for the 20% PEG solution with viscosity ten times greater and flow speeds ten times lower than water, the Péclet number scales as Pe ~ 10^4.

During coalescence, the droplet solution may not reach the bottom of the fluid stripe, making the maximum concentration along a gradient less than that of the droplet solution. This effect was quantified by comparing the maximum intensity in a gradient stripe with that in a fluid stripe of the same total volume but filled entirely with droplet solution (i.e., at a constant concentration: see SI, Section III.2). The ratio of the maximum concentration in the gradient stripes ranged from 90% to 100% of the concentration of the droplet solution and increased with the volume ratio (SI, Figure S7D). Therefore, the droplets were almost fully immersed, which was not surprising since the drop diameters (≈2 mm) were much larger than the depth of the prewet fluid stripes ($H \approx$ 200 μm).

The lateral diffusive smoothing of soluble gradient profiles is illustrated in a sequence of top-down fluorescent images in **Figure 4**Ai: profiles initially have pointed tips which are smoothed over minutes. Since fluorescence intensity is proportional to fluid depth and concentration, the concentration was extracted from measured intensity profiles by dividing by the intensities at corresponding locations on a fluid stripe with constant concentration (SI, Figure S1C). The correction could also have been done by dividing by the depth of the appropriate cylindrical cross-section. The lateral concentrations equilibrate rapidly over minutes (Figure 4Aii); the relaxation was quantified by the standard deviation of the concentration across lateral cross-sections of the gradient (Figure 4Aiii). The standard deviation decreased exponentially in time at rates of 0.0056 and 0.0036 s^{-1} for rhodamine and fluorescein isothiocyanate (FITC)–dextran, respectively, similar to the corresponding theoretical diffusion rates $\pi^2 D/(W/2)^2 = 0.0043$ and 0.0013 s^{-1}. The measured rates were somewhat larger than the theoretical values, perhaps due to the shape of the cross-section: molecules diffuse outward into the shallower edges of the fluid stripe.

The gradient profile was tracked over 24 h to assess its stability. The profiles were within 10% of each other over the first 6 h, and within 20% of each other over the full 24 h period (Figure 4B). During this time period, the gradient stripe was kept in a humid Petri dish to avoid evaporation.

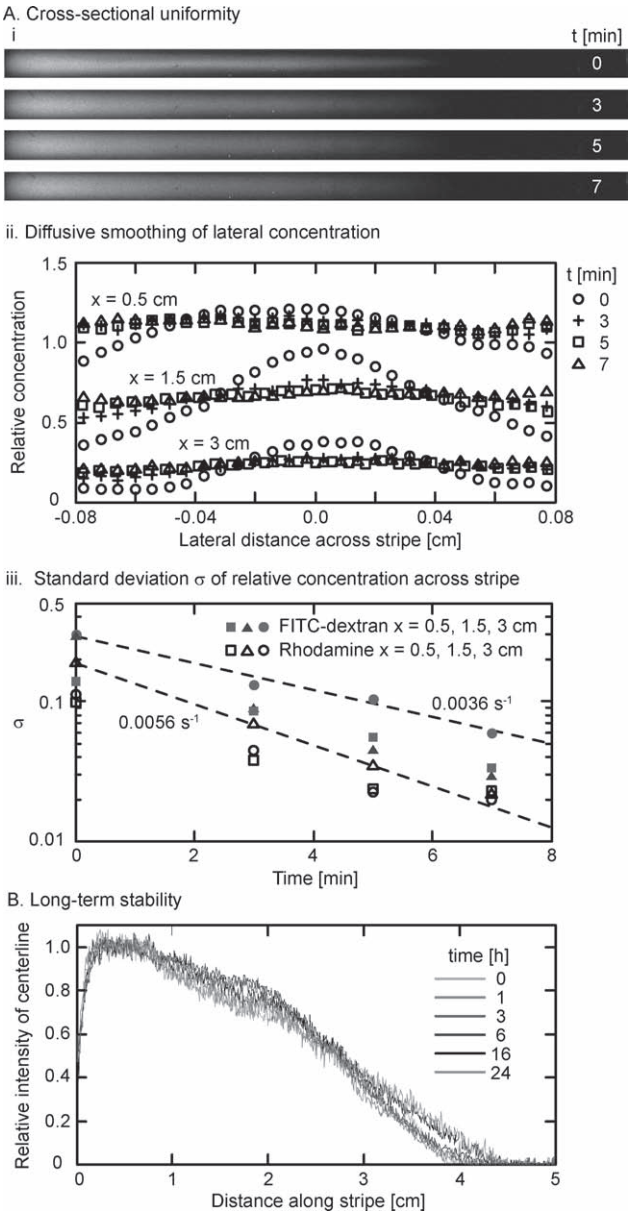

Figure 4. Effects of diffusion on gradient lateral uniformity and stability. A) i) Top-down views of fluorescent droplet plumes containing rhodamine after 0, 3, 5, 7 min following 8 μL droplet addition on 15 μL prewet stripe, showing an increase in lateral uniformity with time; ii) concentration profiles at different lateral cross-sections along fluid stripe. Diffusion smoothes the initially nonuniform lateral profiles in minutes. iii) Standard deviation of intensity along lateral cross-sections decreases exponentially with time, for both rhodamine and fluorescein isothiocyanate (FITC)–dextran solutions. Numbers adjacent to dashed lines indicate slope. B) Stability of gradient profile over 24 h. Profiles become more linear over time and are within 10% of each other over 6 h and within 20% over 24 h.

The observed long-term stability was due to the long timescale for diffusion which scales as $l^2/(\pi^2 D)$, where l is the diffusion length and D the molecular diffusivity. In this study, $D \approx 10^{-6}$ cm^2 s^{-1} and the timescale for diffusion across a distance of $l = 1$ cm is 10^5 s or about 1 day.

2.4. Microparticle Gradients

Micro/nanoparticle gradients have been used to control surface morphology to regulate cell behavior[19] and may also be useful for varying the spatial distribution of degradable particles for the controlled release of drugs. In addition, spatial gradients in cell density are potentially useful for generating biomimetic tissue constructs (e.g., cartilage tissue).[20] Particle gradients have been created by dip-coating/sintering[21] and also by convection in a channel.[6] To create gradients of sedimenting particles by convection in a horizontal channel, high flow speeds must be employed to create the gradient before the particles settle to the bottom.[6] Due to the high speeds generated when a drop is added to the fluid stripe, the current platform is also ideal for creating gradients of microparticles (**Figure 5**A) and cross-gradients of two types of microparticles (Figure 5B). For example, performing the gradient protocol with an 8 μL droplet containing microparticles generated a long, tapered particle-deposition pattern, similar to the initial dye plumes (Figure 5Ai). The centerline concentration profile was somewhat rounded, while the laterally averaged concentration decreased linearly (Figure 5Aiii). Following droplet addition, the particles were allowed to settle for 5 min. To create a cross-gradient of two types of microparticles, 8 μL of fluid (not containing particles) was then removed over 10 s from the opposite end of the stripe and a droplet of the second microparticle solution was added, creating overlapping concentration gradients (Figure 5B). The effect of the flow on the settled microparticles was negligible due to the viscous nonslip condition at the bottom.

The physical mechanisms shaping the particle concentration profiles include the surface-tension driven flow, gravitational settling, and shear-modulated inertial effects on the particles. For similar Reynolds numbers (≈50) and micrometer particle sizes, the latter effect has been shown to move particles toward the centers of the wide sides of high-aspect-ratio straight rectangular channels.[22] Though the flows in and the shapes of our fluid stripes are more complex, the fluid stripes themselves have high aspect ratios, and these inertial effects likely contribute to the observed tapered particle pattern. In contrast, gravitational settling is negligible during the ≈1 s flow: the 10 μm particles with 1.05 g mL^{-1} density used in these experiments settle at approximately 3 μm s^{-1} in distilled water.[6] Gradients of smaller particles, which settle more slowly, could be similarly generated, as in microchannels.[6] As the particle size increases, settling, inertial effects, and effects on the flow profile could become significant.

2.5. Gradient Stripe on a Microwell Array

The fabrication and gradient protocols presented here may be integrated with microwell arrays to deliver soluble and insoluble particle gradients to seeded cells. Microwell arrays were fabricated by existing methods.[23] The gradient stripe was added on top using the same fabrication protocol (mask, spray, dry, remove mask) used for glass slides, and aligned with the rows of microwells (**Figure 6**A).

small NANO MICRO

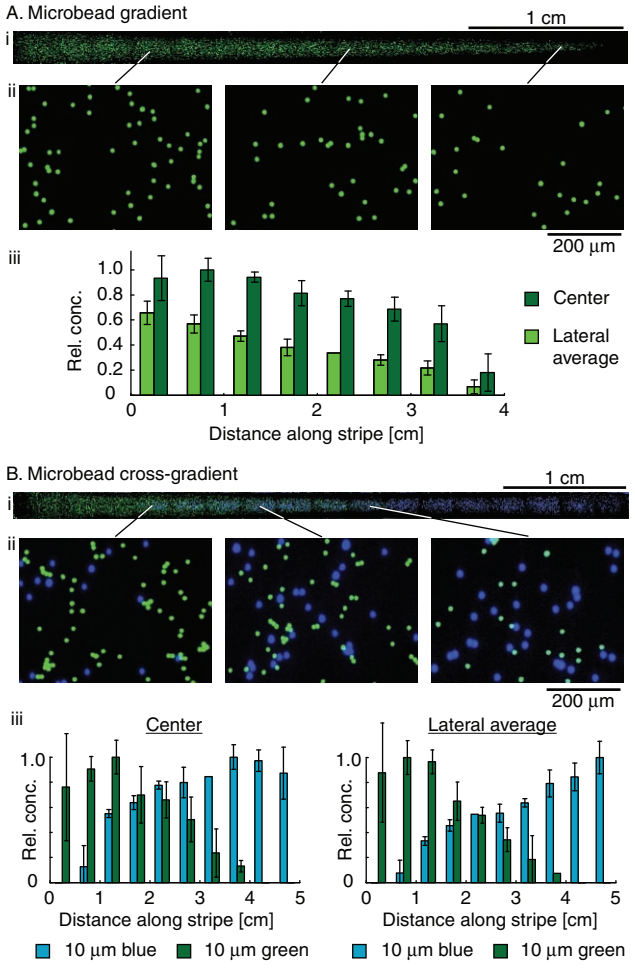

Figure 5. Microparticle gradients. A) i) Stitched top-down view of gradient of 10 µm green fluorescent microparticles delivered by an 8 µL droplet; ii) zooms shown along gradient; iii) centerline and laterally averaged particle concentrations along gradient. B) i) Top-down view of cross-gradient of 10 µm particles created by adding an 8 µL droplet of blue fluorescent particles, removing 8 µL of fluid, and then adding an 8 µL droplet containing green fluorescent particles; ii) zooms shown along gradient; iii) centerline and laterally averaged particle concentrations along channel. In (A,B), intensity levels of displayed microscope images have been increased to visualize particles. Standard deviations greater than 3% shown by error bars. Periodic patterns in (Ai), (Bi) due to nonuniform lighting in stitched microscope images. Rel. conc. = relative concentration.

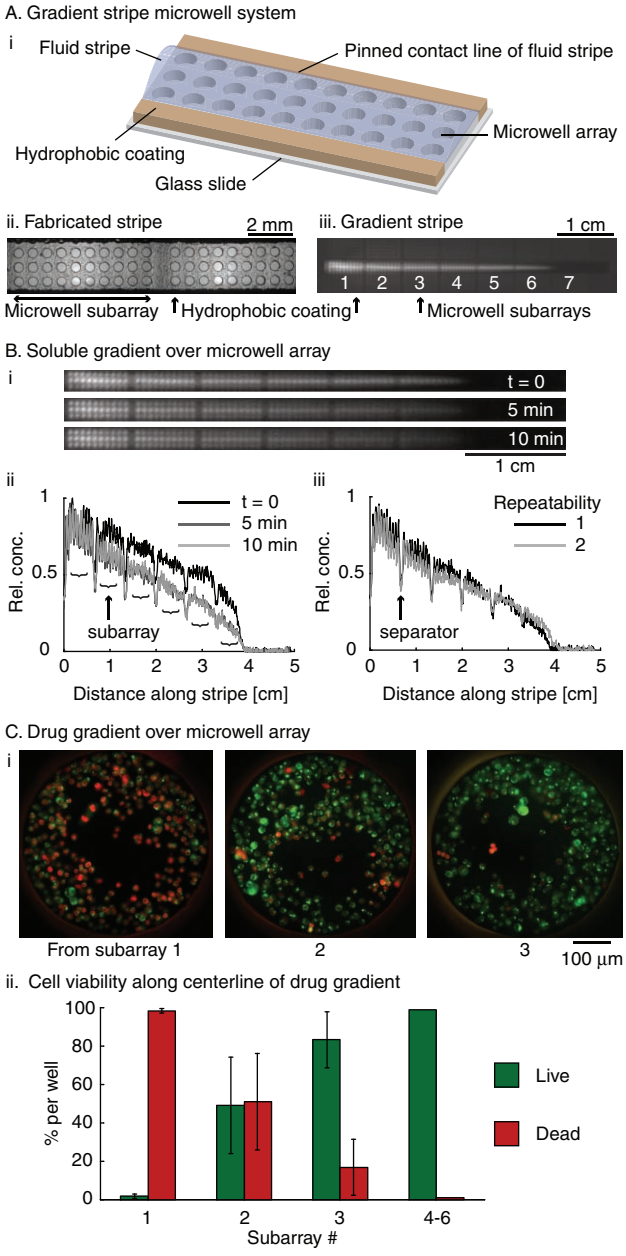

Figure 6. Gradient stripe microwell system. A) i) Schematic; ii) portion of fabricated system; iii) soluble gradient over microwell array, with indexed subarrays. B) i) Top-down views of fluorescent dye gradient after 0, 5, 10 min demonstrating diffusive lateral smoothing; ii) relative centerline concentration over microwells. Wavy profiles due to depth variation between microwells and array surface: subarrays and separators noted; iii) gradient repeatability, after 10 min. D) Drug gradient over microwells leads to a gradient in cell viability: i) 20× composite fluorescent images of Live/Dead assay. Only cells that stained green were counted as live, while those that stained red (regardless of green staining) were counted as dead. ii) Quantification of the cell-viability gradient across the array in terms of subarray index. Intensity levels of microscope images shown in figure have been increased to visualize cells. Error bars indicate standard deviations greater than 1%.

To produce soluble gradients, the microwells were first filled with liquid (containing cells or particles) so that the liquid level was flush with the tops of the microwells. The gradient protocol then proceeded as before: a prewet volume was added on top and a drop of solution was added at one end of the fluid stripe. The results of tests with drops of fluorescent dye are shown in Figure 6B. The intensity was higher over the microwells where the local depth was greater (intensity being proportional to both concentration and fluid depth). Diffusion smoothed the gradient laterally (Figure 6Bi,ii). Reproducible and relatively linear concentration gradients were generated over the microwells along the stripe (Figure 6Biii).

Cell seeding was accomplished by pipetting a drop of cell solution on top of the array and allowing the cells to settle into the wells. Due to the cylindrical shape of the fluid stripe, more cells were seeded in the center wells where the fluid

was deeper. The variable seeding density could therefore be controlled by the cell concentration and the volume of the fluid stripe. Uniform seeding density could be achieved by other standard methods, e.g., by wiping[24] or by immersing the entire slide in cell solution.

Finally, as a proof of concept, we have used our gradient platform and protocol to apply a gradient of the drug doxorubicin to MCF-7 cells seeded within a microwell array. After exposure to the drug, cells exhibited a gradient in viability (Figure 6C). We envision that our simple protocol of adding a gradient stripe on top of microwell arrays to create soluble or particle gradients could find ample use in the biomedical field. Future cell-based experiments could include drug gradients for cell toxicity testing, adhesion-ligand gradients for cell attachment studies, or growth-factor gradients for studies on cell proliferation, chemotaxis, and polarization.[25]

2.6. Additional Remarks

We have outlined a simple method employing passive mechanisms to produce gradients of particles and chemicals directly on a slide in under a second in relatively nonviscous solutions. The fluid stripe was held in place on the hydrophilic stripe by a hydrophobic boundary that pinned the contact line. A droplet added at one end of the stripe coalesced and the resulting disturbance in curvature pressure drove the flow, damped by viscosity, until a new equilibrium state was established. We have also integrated the technique with microwell arrays. Coated slides and microwell arrays with parallel stripes could also be designed for high-throughput testing (SI, Figure S9). The gradient-stripe method is easy to modify and extend, either in-house or with custom-designed, commercially coated slides.

Gradients produced on the stripe are created in open air directly on a glass slide or microwell array, and are therefore easily accessible for later processing and analysis. This ease-of-access permitted visualization of the microparticle gradients immediately after creation, and allowed cell culturing directly on the device prior to applying the drug gradient. Unlike channel-based methods, no microfluidic system was involved in gradient creation. Further processing steps could include cross-linking to form gradient hydrogels.

The dimensions of the gradient stripe were chosen to obtain the longest and most uniform gradients with ample cross-sectional width to cover multiple rows of microwells or repeated conditions for cell exposure. For gradients of soluble materials, diffusion could still laterally smooth the gradients across the 2 mm width in minutes. Also, for the same fluid depth, the radius of curvature scales as W^{-2} (from Equation 1), making wider fluid stripes more flat. Commercially coated slides may be obtained with narrower stripes, or a laser cutter could cut narrower tape masks. Shorter stripes could be used in compact devices.

Lastly, the requirements of the hydrophobic coating are that it pins the contact line of the fluid and holds the fluid stripe in place during droplet addition, rest periods, and device transport. To pin the contact line, the contact angle between the fluid and the hydrophilic stripe should not exceed the advancing contact angle of the hydrophobic coating. For the fluid volumes used here, the contact angles were typically ≈20° to 30° (SI, Section I) for static stripes, although they could reach much larger values at the location of and during droplet addition. The hydrophobic coating used in this paper (WX2100) has an advancing contact angle between 115° and 125°.[26] Other hydrophobic coatings offer similar advancing contact angles and could be used for coating the slides.[27] In fact, tape, sufficiently hydrophobic and properly bonded to the glass slide, could also presumably act as a boundary. A rectangular section could be cut out of the tape and act as the hydrophilic stripe: the contact line of the fluid would be pinned at the edge of the cut-out.

3. Conclusion

In this study we presented a simple yet versatile method of rapidly generating centimeter scale gradients of relatively nonviscous solutions carrying species from the molecular to the micrometer scale. The bench-top fabrication and gradient protocols presented here require only pipettes, glass slides, tape, and hydrophobic spray. The technique is also compatible with microwell arrays, fluorescent cameras and scanners, and microscopes, and is therefore extendable to high-throughput screening and cell-based experiments. The combined experimental characterization and theoretical modeling provide ample design criteria for future applications. The availability of commercially custom-coated slides and the ability to rapidly prototype such slides in-house makes the technique accessible to virtually anyone. We hope that our inexpensive and simple bench-top method further reduces the barriers to generating microfluidic gradients.

4. Experimental Section

Materials: Hydrophobic WX2100 spray (Cytonix Corp., Beltsville, MD), precleaned microscope glass slides (Fisher Scientific, Waltham, MA), poly(ethylene glycol) diacrylate (MW 258 and 4000, Monomer–Polymer & Dajac Labs, Trevose, PA), green fluorescent polymer 10 μm microspheres (1 wt% solids, Duke Scientific Corp., Palo Alto, CA), Fluoresbrite carboxy BB 10 μm microspheres (2.68 wt% solids, Polysciences, Warrington, PA), Live/Dead Viability/Cytotoxicity Kit (Invitrogen, Carlsbad, CA). Michigan Cancer Foundation-7 (MCF-7) cells and Dulbecco's Modified Eagle Medium (DMEM, Invitrogen, CA) were supplemented with 0.1 g mL^{-1} fetal bovine serum and 0.01 g mL^{-1} penicillin–streptomycin. All other reagents were purchased from Sigma–Aldrich (St. Louis, MO), unless otherwise noted.

Coated Slide Fabrication: A glass slide was masked with a 2 mm × 50 mm strip of 3M Magic tape cut with a sharp knife. Hydrophobic spray (WX2100) was applied and allowed to dry for 2 days. The tape mask was then removed. Slides with custom-coated hydrophobic regions may be purchased directly from the manufacturer (e.g., Cel-Line Brand Specialty Printed Slides and Multi-Well Slides with custom coatings from Thermo Scientific's Slides and Specialty Glass division, Portsmouth, NH).

NANO MICRO small

Gradient Protocol: A fluid stripe was formed by pipetting a given "prewet volume" of one solution along a plasma-treated hydrophilic stripe of a coated slide. Plasma cleaning had no noticeable effect on the hydrophobic region. A drop of a second solution containing the salient molecules or particles was added by first secreting and suspending the full droplet from a pipette tip and then bringing the drop in contact with the center of one end of the fluid stripe (Figure 1D). The device was kept in a humid Petri dish (with wet towel) to avoid evaporation. The device was not agitated or moved during droplet addition, rest periods, or image capture. Thus, the gradient protocol was carried out within a Petri dish on the microscope stage, within the fluorescent camera enclosure, or on the lab bench. Following droplet addition, the lid of the Petri dish was replaced carefully to avoid agitation. Videos of this technique are available on request.

Flow Speed Experiments: The gradient protocol was carried out with prewet solutions containing 1X Dulbecco's Phosphate Buffered Saline (DPBS) solution with either 5%, 10%, or 20% (0.05, 0.1, or 0.2 g mL^{-1}, respectively) PEG 4000. Droplets of Trypan blue solution containing the same% PEG as the prewet solution were pipetted onto one end of the fluid stripe. Subsequent fluid motion was recorded by camcorder at 25 frames per second (fps, DPBS-only experiments) or 30 fps (DPBS+PEG experiments) and the dye-tip position was measured in successive frames. Each experiment was repeated three times. The viscosities of the various concentrations of PEG 4000 at 25°C are $\mu = 0.017, 0.029, 0.11$ g cm^{-1} s^{-1} for 5%, 10%, 20% respectively.[18]

Soluble Material Gradient-Profile Experiments: The gradient protocol was carried out with a prewet solution of DPBS, DMEM, or a solution of DPBS containing 5%, 10% or 20% (0.05, 0.1, or 0.2 g mL^{-1}, respectively) PEG 4000. Drops consisted of the prewet solution plus either 0.001 g mL^{-1} Rhodamine 123 (R8004) or 0.01 g mL^{-1} fluorescein isothiocyanate–dextran (FITC–dextran, MW 10 kDa). The diffusion coefficient of FITC–dextran in water at 25°C is[6] $D = 1.3\times10^{-6}$ cm^2 s^{-1}, while that for Rhodamine 123 is[28] $D = 4.4\times10^{-6}$ cm^2 s^{-1}. Fluorescence images were captured with a Kodak Gel Logic 100 Imaging System with 0.8 s exposure time. The fluorescence intensity along the stripe was quantified by ImageJ and Matlab.

Microparticle Gradients: Microparticle stock solutions containing 10 μm-diameter blue or green fluorescent microspheres were diluted 50 and 20 times in DPBS, respectively. To form a single particle gradient, an 8 μL drop of microparticle solution was pipetted onto a 15 μL DPBS fluid stripe. Images were captured along the length of the stripe with a fluorescence microscope (Nikon, USA) with 4× or 10× objectives, and quantified with ImageJ. To create the microparticle cross-gradient, a single gradient was first formed with an 8 μL drop of blue microparticles. The particles were allowed to settle for 5 min. At the opposite end, 8 μL of clear fluid was removed by pipette and an 8 μL drop of green microparticle solution was added. The single and cross-gradient experiments were repeated three and two times, respectively. Measurements were taken from one or two locations within each 0.5 cm interval along stripe. Centerline measurements include particle counts within 0.35 mm of the stripe center. To avoid agitation, the protocol was carried out on the microscope stage and the device was carefully moved horizontally along the stage to capture images.

Gradient Stripe Microwell System and Drug Gradient: Microwells with 400 μm diameter, 100 μm depth, and 600 μm center spacing were fabricated from PEG 258 with polydimethylsiloxane (PDMS) stamps according to a previous protocol.[23] The coating protocol outlined above was then applied on top of the microwell array layer. The device was cleaned with 100% alcohol for 2 h, sterilized with 75% alcohol, washed with DPBS five times and air dried. The total volume of the microwells was 2.6 μL (seven 3 × 10 microwell subarrays, see Figure 6C). Fluorescent gradients over empty wells were formed by prewetting the stripe and microwells with 17.5 μL DPBS; approximately 15 μL of prewet fluid remained above the wells.

To form the drug gradient over cells, the stripe and microwells were soaked with 40 μL of 0.002 g mL^{-1} gelatin solution, incubated for 6 h, washed by DPBS and air dried, prewet with 50 μL of MCF-7 cell suspension (1.0×10^5 cells mL^{-1}) and cultured for 12 h. The unattached cells were aspirated and the excess fluid above the microwells removed. The gradient protocol was carried out with 15 μL of fresh culture medium (prewet solution) and an 8 μL droplet of 50 μM doxorubicin solution. The device was incubated and not agitated for 6 h. The drug solution was then removed and replaced by 50 μL of Live/Dead solution. After 10 min, 20× images were taken with a fluorescence microscope and quantified with ImageJ's cell counter. A pixel intensity threshold of 20 (out of 255) was used as a lower cutoff to determine if a cell was stained red or green. Only cells that stained green were counted as live, while those that stained red (regardless of green staining) had damaged outer walls and were counted as dead.[29] Results from each subarray were averaged over a total of at least 4 microwells from two repeated experiments.

Supporting Information

Supporting Information is available from the Wiley Online Library or from the author.

Acknowledgements

All authors planned the research. MJH designed the coated slide-top device, developed the theoretical models, and wrote the paper. JH and MJH developed the experimental protocols. JH performed all experiments. MJH and JH processed and analyzed the data. MJH and JH contributed equally as lead authors. AK supervised the research. All authors revised the manuscript and agreed on its final contents. This research was funded by the NIH (HL092836, DE019024, EB007249), the Office of Naval Research, the US Army Corps of Engineers, and the National Science Foundation CAREER award (AK). JH was partially sponsored by the China Scholarship Council (CSC), National High Technology Research and Development Program (2009AA043801), China. We thank Nina Sinatra for help with preliminary experiments during her Undergraduate Research Opportunity Program training experience. We thank Dr. Gulden Camci-Unal, Francesco Piraino, and Wenqian Xiao for technical help, and Prof. John Bush, Dr. Yanan Du, Dr. Nezam Kachouie, Ben Wang, and Dr. Hirokazu Kaji for useful comments.

[1] a) J. Genzer, R. R. Bhat, *Langmuir* **2008**, *24*, 2294; b) T. M. Keenan, A. Folch, *Lab Chip* **2008**, *8*, 34; c) S. Sant, M. J. Hancock, J. P. Donnelly, D. Iyer, A. Khademhosseini, *Can. J. Chem. Eng.* **2010**, *88*, 899; d) S. Kim, H. J. Kim, N. L. Jeon, *Integr. Biol.* **2010**, *2*, 584.
[2] S. K. W. Dertinger, D. T. Chiu, N. L. Jeon, G. M. Whitesides, *Anal. Chem.* **2001**, *73*, 1240.
[3] S. A. DeLong, J. J. Moon, J. L. West, *Biomaterials* **2005**, *26*, 3227.
[4] J. Goulpeau, B. Lonetti, D. Trouchet, A. Ajdari, P. Tabeling, *Lab Chip* **2007**, *7*, 1154.
[5] Y. Du, J. Shim, M. Vidula, M. J. Hancock, E. Lo, B. G. Chung, J. T. Borenstein, M. Khabiry, D. M. Cropek, A. Khademhosseini, *Lab Chip* **2009**, *9*, 761.
[6] Y. Du, M. J. Hancock, J. He, J. L. Villa-Uribe, B. Wang, D. M. Cropek, A. Khademhosseini, *Biomaterials* **2010**, *31*, 2686.
[7] a) J. Atencia, D. J. Beebe, *Nature* **2005**, *437*, 648; b) J. Berthier, P. Silberzan, *Microfluidics for Biotechnology*, Artech House, Norwood, MA**2006**; c) C. D. Chin, V. Linder, S. K. Sia, *Lab Chip* **2007**, *7*, 41; d) W. G. Lee, Y. G. Kim, B. G. Chung, U. Demirci, A. Khademhosseini, *Adv. Drug Deliver. Rev.* **2010**, *62*, 449.
[8] A. W. Martinez, S. T. Phillips, G. M. Whitesides, *Proc. Natl. Acad. Sci. USA* **2008**, *105*, 19606.
[9] a) X. Zhu, L. Y. Chu, B. Chueh, M. Shen, B. Hazarika, N. Phadke, S. Takayama, *Analyst* **2004**, *129*, 1026; b) G. M. Walker, D. J. Beebe, *Lab Chip* **2002**, *2*, 131; c) D. Juncker, H. Schmid, U. Drechsler, H. Wolf, M. Wolf, B. Michel, N. de Rooij, E. Delamarche, *Anal. Chem.* **2002**, *74*, 6139.
[10] S. A. Zawko, C. E. Schmidt, *Lab Chip* **2010**, *10*, 379.
[11] J. He, Y. Du, J. L. Villa-Uribe, C. Hwang, D. Li, A. Khademhosseini, *Adv. Funct. Mater.* **2010**, *20*, 131.
[12] K. A. Wier, L. C. Gao, T. J. McCarthy, *Langmuir* **2006**, *22*, 4914.
[13] B. Zhao, J. S. Moore, D. J. Beebe, *Science* **2001**, *291*, 1023; b) P. Lam, K. J. Wynne, G. E. Wnek, *Langmuir* **2002**, *18*, 948; c) N. M. Oliveira, A. I. Neto, W. Song, J. F. Mano, *Appl. Phys. Express* **2010**, *3*, 5205; d) C. S. Oh, *United States Patent 5,904,824*, **1999**.
[14] R. L. Speth, E. Lauga, *New J. Phys.* **2009**, *11*, 075024.
[15] a) H. Gau, S. Herminghaus, P. Lenz, R. Lipowsky, *Science* **1999**, *283*, 46; b) R. V. Roy, L. W. Schwartz, *J. Fluid Mech.* **1999**, *391*, 293; c) R. A. Brown, L. E. Scriven, *J. Colloid Interface Sci.* **1980**, *78*, 528; d) G. D. Towell, L. B. Rothfeld, *AIChE J.* **1966**, *12*, 972.
[16] S. H. Davis, *J. Fluid Mech.* **1980**, *98*, 225.
[17] F. Blanchette, T. P. Bigioni, *Nat. Phys.* **2006**, *2*, 254.
[18] a) S. Kirincic, C. Klofutar, *Fluid Phase Equilib.* **1999**, *155*, 311; b) P. Gonzalez-Tello, F. Camacho, G. Blazquez, *J. Chem. Eng. Data* **1994**, *39*, 611.
[19] T. P. Kunzler, C. Huwiler, T. Drobek, J. Vörös, N. D. Spencer, *Biomaterials* **2007**, *28*, 5000.
[20] T. B. F. Woodfield, C. A. V. Blitterswijk, J. D. Wijn, T. J. Sims, A. P. Hollander, J. Riesle, *Tissue Eng.* **2005**, *11*, 1297.
[21] C. Huwiler, T. P. Kunzler, M. Textor, J. Vörös, N. D. Spencer, *Langmuir* **2007**, *23*, 5929.
[22] A. A. S. Bhagat, S. S. Kuntaegowdanahalli, I. Papautsky, *Phys. Fluids* **2008**, *20*, 101702.
[23] H. C. Moeller, M. K. Mian, S. Shrivastava, B. G. Chung, A. Khademhosseini, *Biomaterials* **2008**, *29*, 752.
[24] L. Kang, M. J. Hancock, M. D. Brigham, A. Khademhosseini, *J. Biomed. Mat. Res. A* **2010**, *93*, 547.
[25] A. Shamloo, N. Ma, M. Poo, L. L. Sohn, S. C. Heilshorn, *Lab Chip* **2008**, *8*, 1292.
[26] J. M. Aristoff, T. T. Truscott, A. H. Techet, J. W. M. Bush, *Phys. Fluids* **2010**, *22*, 032102.
[27] a) C. L. Bower, E. A. Simister, K. Paul, *J. Phys. D: Appl. Phys.* **2008**, *41*, 174002; b) W. Song, D. D. Veiga, C. A. Custódio, J. F. Mano, *Adv. Mater.* **2009**, *21*, 1830.
[28] P. O. Gendron, F. Avaltroni, K. J. Wilkinson, *J. Fluoresc.* **2008**, *18*, 1093.
[29] N. G. Papadopoulos, G. V. Z. Dedoussis, G. Spanakos, A. D. Gritzapis, C. N. Baxevanis, M. Papamichail, *J. Immunol. Methods* **1994**, *177*, 101.

Received: November 20, 2010
Published online:

